Euro. Jnl of Applied Mathematics (2021), *vol.* 32, *pp.* 199–225 © The Author(s), 2020. Published by Cambridge University Press.
doi:10.1017/S0956792520000091

On small-time similarity-solution behaviour in the solidification shrinkage of binary alloys†

M. ASSUNÇÃO[1], M. VYNNYCKY[2] and S.L. MITCHELL[2]

[1]*Department of Applied Mathematics and Statistics, Institute of Mathematical and Computer Sciences, University of São Paulo at São Carlos, PO Box 668, São Carlos, 13560-970 SP, Brazil*
email: assuncao@icmc.usp.br
[2]*Department of Mathematics and Statistics, University of Limerick, Limerick V94 T9PX, Ireland*

(*Received 15 March 2019*; *revised 17 March 2020*; *accepted 19 March 2020*; *first published online 17 April 2020*)

In the one-dimensional solidification of a binary alloy undergoing shrinkage, there is a relative motion between solid and liquid phases in the mushy zone, leading to the possibility of macrosegregation; thus, the problem constitutes an invaluable benchmark for the testing of numerical codes that model these phenomena. Here, we revisit an earlier obtained solution for this problem, that was posed on a semi-infinite spatial domain and valid for the case of low superheat, with a view to extending it to the more general situation of a finite spatial domain, arbitrarily large superheat and both eutectic and non-eutectic solidification. We find that a similarity solution is available for short times which contains a boundary layer on the liquid side of the mush–liquid interface; this solution is believed to constitute the correct initial condition for the subsequent numerical solution of the full non-similar problem, which is deferred to future work.

Key words: Moving boundary problems, dynamics of phase boundaries, dimensional analysis and similarity

2020 Mathematics Subject Classification: 76M55 (Primary); 74N20 (Secondary)

1 Introduction

Although highly idealised, the one-dimensional problem for the solidification of a cooling binary alloy melt which simultaneously undergoes solidification shrinkage is important for a number of reasons. In this situation, a melt velocity is induced and this is therefore the simplest configuration in which to examine the role of convection in a binary system. Moreover, this configuration is believed to permit a similarity solution to the governing equations [8, 18, 31, 40], which can then be used as a benchmark for testing higher dimensional numerical codes. Furthermore, the fact that there is a relative motion between solid and liquid phases in the so-called mushy zone, where the two phases coexist, leads to the possibility of macrosegregation [9, 13, 14, 22, 26], that is, variations in composition that occur in alloy castings or ingots and range in scale from several

† The first author acknowledges the financial support of Fundação de Amparo à Pesquisa do Estado de São Paulo (FAPESP) for the researcher grant (grant number 2016/12678-0). The second author acknowledges the financial support of FAPESP for the award of a visiting researcher grant (grant number 2018/07643-8).

https://doi.org/10.1017/S0956792520000091 Published online by Cambridge University Press

millimetres to centimetres or even metres; this is a central problem in industry, since it strongly influences the further workability of the cast products and their mechanical properties.

The main of focus of this paper is to extend the similarity solution presented in [31] for the problem of a semi-infinite melt being cooled by a boundary that is held at constant temperature; in particular, whereas the problem in [31] was posed on a semi-infinite spatial domain and valid for the case when the solidification was eutectic and the initial temperature of the melt was just above the liquidus temperature of the alloy, that is, low superheat, here we consider the more general situation of a finite spatial domain, arbitrarily large superheat and both eutectic and non-eutectic solidification. Consequently, there cannot be a similarity solution for all time, as was the case in [31]. On the other hand, we find that a similarity solution is available for short times which contains a boundary layer on the liquid side of the mush–liquid interface; subsequently, this solution would constitute the correct initial condition for the numerical solution of the full non-similar problem, which is deferred to future work. Moreover, it should be strongly emphasised that this problem is fundamentally different from others, such as those in [6, 16], involving the solidification of a binary melt. The difference lies in the fact that the latter are problems in which the solidification front may still be planar, having not yet undergone the Mullins–Sekerka instability [27]; as a consequence, the problems treated in [6, 16] contain a solid phase, a molten phase and a moving interface between them. On the other hand, the problem in [31] is posed for the situation where the Mullins–Sekerka instability has already occurred and considered a representative elementary volume containing many solid dendrites that coexist with interdendritic melt. This region is referred to as the mushy zone, and it is mathematically convenient to treat the overall problem as one containing three regions, that is, solid, mush and liquid, with the three being separated by moving solid–mush and mush–liquid interfaces.

The layout of the paper is as follows. In Section 2, we formulate and non-dimensionalise the governing equations. A triple Landau transformation is used in Section 3 to reformulate the equations, which are then analysed in the small-time limit, leading to a system of similarity ordinary differential equations (ODEs); the solutions to these, which must be obtained numerically, are presented in Section 4. Conclusions are drawn in Section 5. In addition, three appendices serve to demonstrate how the formulation links naturally to the conservation of momentum for this problem, which is otherwise absent from the foregoing analysis, show how the boundary layer mentioned above would also be present in an earlier model for the solidification of a sphere [21] and provide a quantitative comparison with the results in [31].

2 Mathematical formulation

We consider a transient one-dimensional problem, as shown in Figure 1, in which a region of binary alloy melt of initial extent l, temperature T_{cast} and composition C_0 is cooled by a boundary at $y = 0$ that is held at temperature T_{w}. To fix ideas more precisely, we suppose that the alloy in question has a phase diagram with a eutectic point, with eutectic temperature and concentration T_{eut} and C_{eut}, respectively, as indeed is the case for many alloys of technological interest. Figure 2 shows the phase diagram for the Al–Cu system, which was the one implicitly considered by [31] and the one that we will consider here, and we will also assume that $T_{\text{w}} < T_{\text{eut}}$, which ensures that complete solidification occurs for any choice of C_0, such that $0 \leqslant C_0 \leqslant C_{\text{eut}}$. As indicated in Figure 1, at some time $t > 0$, the region that initially occupied $0 \leqslant y \leqslant l$ will shrink to occupy $0 \leqslant y \leqslant y_\infty(t)$, which consists of a solid region occupying $0 \leqslant y \leqslant y_{\text{s}}(t)$, a mushy zone occupying

https://doi.org/10.1017/S0956792520000091 Published online by Cambridge University Press

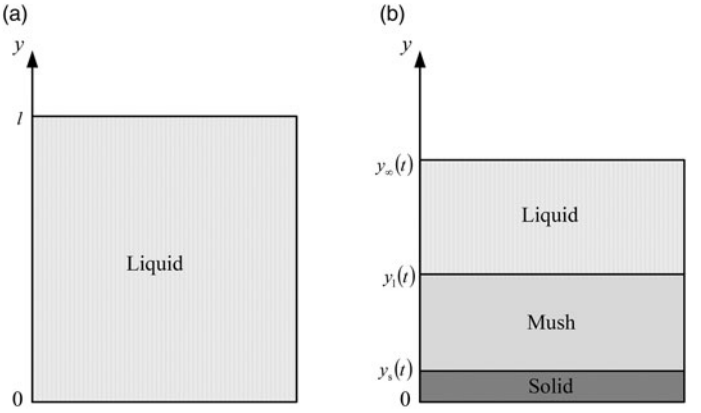


FIGURE 1. Solidification with shrinkage: (a) initial configuration at $t = 0$ and (b) after time $t > 0$.

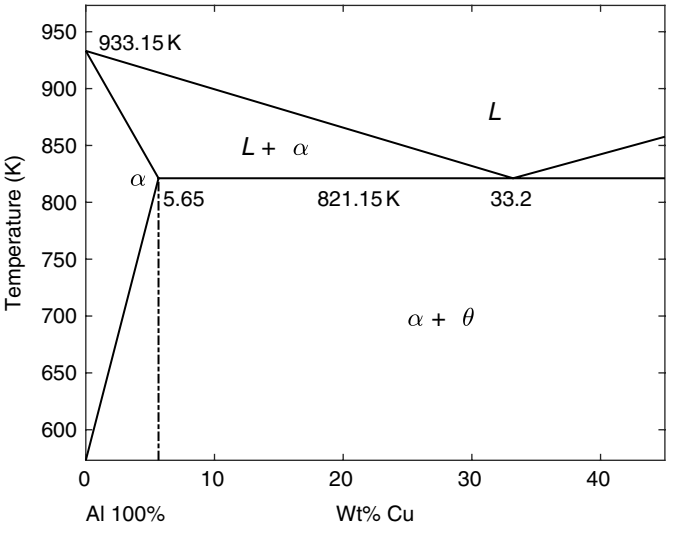


FIGURE 2. Al-rich side of the linearised phase diagram for the Al–Cu system. L denotes liquid phase, and α and θ denote two solid phases.

$y_s(t) \leqslant y \leqslant y_l(t)$ and the melt region occupying $y_l(t) \leqslant y \leqslant y_\infty(t)$; the shrinkage occurs as a result of phase change, as molten melt begins to solidify, with the density of the solid being greater than that of the molten phase. We consider the governing equations for each region in turn.

2.1 Governing equations

2.1.1 *Solid region,* $0 \leqslant y \leqslant y_s(t)$

The only equation is that for the conservation of energy, following the Fourier's second law with no internal generation and assuming constant material properties [1, 7], which is given by

$$\rho_s c_{ps} \frac{\partial T}{\partial t} = k_s \frac{\partial^2 T}{\partial y^2}, \tag{2.1}$$

https://doi.org/10.1017/S0956792520000091 Published online by Cambridge University Press

where T denotes the temperature, and ρ_s, c_{ps} and k_s the density, specific heat capacity and thermal conductivity, respectively, of the solid phase, all of which are assumed to be constant.

2.1.2 *Mush,* $y_s(t) \leqslant y < y_l(t)$

The total mass balance over solid and liquid phases in the mush, derived from summing the phase conservation equations as in [4], is given by

$$\frac{\partial \rho}{\partial t} + \frac{\partial}{\partial y}(\rho_l \chi v) = 0, \tag{2.2}$$

where ρ_l is the density of the liquid phase, and with the mass-averaged velocity consisting only of the liquid phase velocity, v, since the solid does not move and its velocity is therefore zero. Also, ρ is the mixture density which, following [39], is written in terms of the liquid fraction, χ, as

$$\rho = \chi \rho_l + (1 - \chi)\rho_s; \tag{2.3}$$

equation (2.2) can then be written as

$$(1 - R)\frac{\partial \chi}{\partial t} + \frac{\partial U}{\partial y} = 0, \tag{2.4}$$

where $R = \rho_s/\rho_l$ and $U = \chi v$.

The conservation of energy is given by

$$\frac{\partial}{\partial t}\left(\left\{\rho_l c_{pl}\chi + \rho_s c_{ps}(1 - \chi)\right\}(T - T_{ref})\right) + \frac{\partial}{\partial y}\left(\rho_l c_{pl} U (T - T_{ref})\right)$$
$$= \frac{\partial}{\partial y}\left(k\frac{\partial T}{\partial y}\right) - \Delta H_f \frac{\partial}{\partial t}(\rho_l \chi), \tag{2.5}$$

where c_{pl} and k_l denote the specific heat capacity and thermal conductivity, respectively, of the liquid phase, ΔH_f is the latent heat of fusion and k is the mixture thermal conductivity, given by

$$k = \chi k_l + (1 - \chi)k_s; \tag{2.6}$$

although this is arguably not the most natural mixture rule, which would be based on the reciprocal of conductivities, it is nevertheless one that is frequently used [2,29,39]. Also, T_{ref} is a reference temperature, to which thermal energies in all phases must refer consistently; a convenient choice for T_{ref} is T_m, the melting point of the solvent element.

The equation for the conservation of solute, taken over solid and liquid phases, is given by

$$\frac{\partial}{\partial t}(\rho C) + \frac{\partial}{\partial y}(\rho_l C_l U) = 0, \tag{2.7}$$

where the form for the mixture concentration, C, depends on the assumption made regarding solute transport at the microscale. The two extremes are the lever rule and the Scheil equation [19,28,30,41], where

$$\rho C = \chi \rho_l C_l + \begin{cases} \rho_s (1 - \chi) C_s, & \text{lever rule,} \\ \rho_s \int_0^{1-\chi} C_s \mathrm{d}\chi', & \text{Scheil equation,} \end{cases} \tag{2.8}$$

https://doi.org/10.1017/S0956792520000091 Published online by Cambridge University Press

with C_l and C_s as the concentrations of the solute in the liquid and solid phases, respectively, which are related by

$$C_s = k_0 C_l, \tag{2.9}$$

where k_0 is the partition coefficient; moreover, the lever rule assumes thermodynamic equilibrium between the phases, whereas the Scheil rule, also known as the non-equilibrium lever rule, assumes no solute diffusion in the solid and perfect mixing in the liquid [1]. For the purposes of generalisation, it is possible to introduce a parameter β, where $0 \leqslant \beta \leqslant 1$, that allows for a back-diffusion treatment, that is, partial solute diffusion into the solid, that lies between the limits of zero back diffusion ($\beta = 0$, the Scheil assumption) and complete back diffusion ($\beta = 1$, the lever rule); as indicated in [28], this treatment of back diffusion is equivalent to using the Clyne and Kurz correction [10] of the well-known back-diffusion model of [5]. Following [28] in first setting

$$\int_0^{1-\chi} \frac{\partial C_s}{\partial t} \mathrm{d}\chi' = \beta\,(1-\chi)\,k_0 \frac{\partial C_l}{\partial t}, \tag{2.10}$$

equation (2.7) becomes

$$\rho_l \frac{\partial}{\partial t}\,(\chi C_l) - k_0 \rho_s C_l \frac{\partial \chi}{\partial t} + \rho_s \beta\,(1-\chi)\,k_0 \frac{\partial C_l}{\partial t} + \frac{\partial}{\partial y}\,(\rho_l C_l U) = 0; \tag{2.11}$$

furthermore, we note that (2.8) can now be generalised for $0 \leqslant \beta \leqslant 1$ to

$$\rho C = \chi \rho_l C_l + \rho_s \int_0^{1-\chi} \left(C_s + \beta \chi' \frac{\mathrm{d}C_s}{\mathrm{d}\chi'} \right) \mathrm{d}\chi'. \tag{2.12}$$

We also have local thermodynamic equilibrium in the mushy region, so that, from the liquidus line in the phase diagram,

$$T = T_m - m C_l \quad \text{for } 0 \leqslant \chi \leqslant 1, \tag{2.13}$$

where $m > 0$; note here that, in view of the minus sign in equation (2.13), the slope of the liquidus line in the phase diagram will be $-m$.

Lastly, we note that we have not mentioned any equation for the conservation of momentum; this is discussed in Appendix A.

2.1.3 *Melt region, $y_l(t) \leqslant y \leqslant y_\infty(t)$*

Here, the mass balance can be written as just

$$\frac{\partial U}{\partial y} = 0, \tag{2.14}$$

which can be thought of as the result of setting $\chi = 1$ in equation (2.4).

The conservation of energy is given by

$$\rho_l c_{pl} \left(\frac{\partial}{\partial t}\,(T - T_{ref}) + \frac{\partial}{\partial y}\,(U\,(T - T_{ref})) \right) = k_l \frac{\partial^2 T}{\partial y^2}, \tag{2.15}$$

https://doi.org/10.1017/S0956792520000091 Published online by Cambridge University Press

also derived considering $\chi = 1$ in equation (2.5), while neglecting changes in material properties inside the melt region, whereas the conservation of solute, as in [17], is given by

$$\frac{\partial}{\partial t}(\rho_l C_l) + \frac{\partial}{\partial y}(\rho_l C_l U) = 0. \tag{2.16}$$

For simplicity, we henceforth set $c_{ps} = c_{pl}$ and $k_s = k_l$, although keeping $\rho_s \neq \rho_l$ throughout.

2.2 Boundary and interface conditions

2.2.1 *Heat and solute*

At $y = 0$, we have

$$T = T_w, \tag{2.17}$$

as implied by the discussion at the beginning of Section 2.

We assume negligible heat loss at the upper surface of the melt, which is expressed by

$$\frac{\partial T}{\partial y} = 0 \quad \text{at } y = y_\infty(t). \tag{2.18}$$

Similarly, a condition is necessary on the solute concentration; analogous to (2.18), we take

$$\frac{\partial C_l}{\partial y} = 0. \tag{2.19}$$

We also require interface conditions at $y = y_s(t)$ and $y_l(t)$. At $y = y_s(t)$, two of these – the continuity of temperature and a heat balance – are straightforward and are given, respectively, by

$$[T]^+_- = 0 \quad \text{at } y = y_s(t), \tag{2.20}$$

$$\left[k\frac{\partial T}{\partial y}\right]^+_- = -\rho_l \Delta H_f \chi \frac{dy_s}{dt} \quad \text{at } y = y_s(t), \tag{2.21}$$

with $[\ ]^+_-$ denoting the difference in the value of that function above and below $y = y_s(t)$; note that the value of k on the minus side in (2.21) is implicitly taken to be k_s. The relation (2.21) denotes the Stefan condition, which states that the rate of change in latent heat equals the amount by which the conductive heat flux jumps across the interface [1]. Also, it is evident that the temperature on the mush side of this interface must satisfy (2.13), but this in itself does not provide a third condition, since C_l is not yet known. Considering first the limiting case of eutectic solidification, it is known that one should set $T = T_{eut}$, which will lead to $C_l = C_{eut}$, and that $\chi > 0$ at $y = y_s(t)$; the actual value of χ must be computed as part of the solution. On the other hand, if $C_l < C_{eut}$, then $\chi = 0$ at $y = y_s(t)$; in this case, neither T nor C_l are known *a priori*, although they are linked by (2.13) and must be computed. Moreover, for arbitrary values of the model parameters, it cannot be known beforehand whether C_l at $y = y_s(t)$ will reach C_{eut} or not. In summary, we have

$$\begin{cases} \chi = 0, \quad T = T_m - mC_l, & \text{if } C_l < C_{eut} \\ T = T_{eut}, & \text{if } C_l = C_{eut} \end{cases} \quad \text{at } y = y_s(t), \tag{2.22}$$

https://doi.org/10.1017/S0956792520000091 Published online by Cambridge University Press

indicating that two relations are required for the three dependent variables χ, T and C_l. Furthermore, we shall henceforth set $\chi_\mathrm{s} = \chi|_{y=y_\mathrm{s}(t)}$.

At $y = y_\mathrm{l}(t)$, we have the continuity of temperature and heat flux, so that

$$[T]_-^+ = 0, \tag{2.23}$$

$$\left[k\frac{\partial T}{\partial y}\right]_-^+ = 0, \tag{2.24}$$

where the value of k on the plus side in (2.24) is implicitly taken to be k_l, and, analogous to the first alternative in (2.22),

$$\chi = 1, \quad T = T_\mathrm{m} - mC_\mathrm{l}. \tag{2.25}$$

2.2.2 *Mass*

Boundary conditions for U are obtained by considering the global conservation of mass. For this, we have

$$\rho_\mathrm{s}\int_0^{y_\mathrm{s}(t)} \mathrm{d}y + \int_{y_\mathrm{s}(t)}^{y_\mathrm{l}(t)} \rho \mathrm{d}y + \rho_\mathrm{l}\int_{y_\mathrm{l}(t)}^{y_\infty(t)} \mathrm{d}y = \rho_\mathrm{l}\int_0^{l} \mathrm{d}y, \tag{2.26}$$

which, on rearranging using (2.3), gives

$$(1-R)\left\{\int_{y_\mathrm{s}(t)}^{y_\mathrm{l}(t)} \chi \mathrm{d}y - y_\mathrm{l}(t)\right\} = \int_{y_\infty(t)}^{l} \mathrm{d}y. \tag{2.27}$$

Differentiating (2.27) with respect to t and using Leibniz' rule gives

$$(1-R)\left\{\dot{y}_\mathrm{l}(t)\,\chi\,(y_\mathrm{l}(t)) - \chi_\mathrm{s}\dot{y}_\mathrm{s}(t)\,\chi_\mathrm{s} + \int_{y_\mathrm{s}(t)}^{y_\mathrm{l}(t)} \frac{\partial \chi}{\partial t}\mathrm{d}y - \dot{y}_\mathrm{l}(t)\right\} = -\dot{y}_\infty(t), \tag{2.28}$$

whence

$$(1-R)\left\{\int_{y_\mathrm{s}(t)}^{y_\mathrm{l}(t)} \frac{\partial \chi}{\partial t}\mathrm{d}y - \chi_\mathrm{s}\dot{y}_\mathrm{s}(t)\right\} = -\dot{y}_\infty(t); \tag{2.29}$$

using (2.4) gives

$$(1-R)\left\{\frac{1}{1-R}\int_{y_\mathrm{s}(t)}^{y_\mathrm{l}(t)} \frac{\partial U}{\partial y}\mathrm{d}y + \chi_\mathrm{s}\dot{y}_\mathrm{s}(t)\right\} = 0, \tag{2.30}$$

leading to

$$(U)_{y_\mathrm{s}(t)} - (U)_{y_\mathrm{l}(t)} = (1-R)\,\chi_\mathrm{s}\dot{y}_\mathrm{s}(t) - \dot{y}_\infty(t). \tag{2.31}$$

Moreover, because U is continuous at $y = y_\mathrm{l}(t)$, this will be the value used in (2.2). Note also that U in the melt satisfies

$$\frac{\partial U}{\partial y} = 0, \tag{2.32}$$

https://doi.org/10.1017/S0956792520000091 Published online by Cambridge University Press

and implies that $U = U(t)$ there; furthermore, taking $U \neq 0$ in the melt is consistent with the analogous problem of the melting of a solid block, in which $U \neq 0$ in the as-yet unmelted solid [1]. In fact,

$$(U)_{y_l(t)} = \dot{y}_\infty(t), \tag{2.33}$$

leading to

$$(U)_{y_s(t)} = (1-R)\,\chi_s \dot{y}_s(t). \tag{2.34}$$

2.3 Initial conditions

For $y > 0$,

$$T = T_{\text{cast}}, \tag{2.35}$$

$$C_l = C_0. \tag{2.36}$$

We will also need initial-like conditions for y_l, y_s and y_∞, and we set

$$y_l(0) = 0, \tag{2.37}$$

$$y_s(0) = 0, \tag{2.38}$$

$$y_\infty(0) = l. \tag{2.39}$$

Furthermore, these yield a further condition. Integrating (2.7) over $0 \leqslant y \leqslant y_\infty(t)$, we have

$$\int_0^{y_\infty(t)} \frac{\partial}{\partial t}(\rho C)\,\mathrm{d}y = -\left[\rho_l C_l U\right]_0^{y_\infty(t)}.$$

Applying Leibniz' rule on the left-hand side, we have

$$\int_0^{y_\infty(t)} \frac{\partial}{\partial t}(\rho C)\,\mathrm{d}y = \frac{\partial}{\partial t}\left(\int_0^{y_\infty(t)} \rho C \mathrm{d}y\right) - \dot{y}_\infty(t)\,(\rho C)_{y_\infty(t)},$$

which results in just

$$\frac{\partial}{\partial t}\left(\int_0^{y_\infty(t)} \rho C \mathrm{d}y\right) = 0.$$

Applying the initial conditions, we have

$$\int_0^{y_\infty(t)} \rho C \mathrm{d}y = \rho_l C_0 l; \tag{2.40}$$

note that this describes the conservation of solute over the whole system.

2.4 Non-dimensionalisation

In order to non-dimensionalise the equations, we set

$$Y = \frac{y}{l}, \quad \tau = \frac{t}{[t]}, \quad \theta = \frac{T - T_w}{T_{\text{cast}} - T_w}, \quad \hat{U} = \frac{U}{l/[t]}, \quad Y_s = \frac{y_s}{l}, \quad Y_l = \frac{y_l}{l}, \quad Y_\infty = \frac{y_\infty}{l}, \tag{2.41}$$

https://doi.org/10.1017/S0956792520000091 Published online by Cambridge University Press

where $[t]$ is a timescale, which we shall take as being given by $[t] = \rho_l c_{pl} l^2 / k_l$. In the solid,

$$R \frac{\partial \theta}{\partial \tau} = \frac{\partial^2 \theta}{\partial Y^2}; \tag{2.42}$$

in the mush,

$$\frac{\partial}{\partial \tau} (\chi + (1 - \chi) R) + \frac{\partial \hat{U}}{\partial Y} = 0, \tag{2.43}$$

$$[\chi + (1 - \chi) R] \frac{\partial \theta}{\partial \tau} + \hat{U} \frac{\partial \theta}{\partial Y} = \frac{\partial^2 \theta}{\partial Y^2} - \frac{R}{St} \frac{\partial \chi}{\partial \tau}, \tag{2.44}$$

$$\frac{\partial}{\partial \tau} (\chi C_l) - k_0 R C_l \frac{\partial \chi}{\partial \tau} + \beta R (1 - \chi) k_0 \frac{\partial C_l}{\partial \tau} + \frac{\partial}{\partial Y} \left(C_l \hat{U} \right) = 0, \tag{2.45}$$

$$\theta = \theta_m - \tilde{m} C_l, \tag{2.46}$$

where $St = c_{pl} (T_{cast} - T_w) / \Delta H_f$ and

$$\theta_m = \frac{T_m - T_w}{T_{cast} - T_w}, \quad \tilde{m} = \frac{m}{T_{cast} - T_w};$$

in the melt,

$$\frac{\partial \hat{U}}{\partial Y} = 0, \tag{2.47}$$

$$\frac{\partial \theta}{\partial \tau} + \hat{U} \frac{\partial \theta}{\partial Y} = \frac{\partial^2 \theta}{\partial Y^2}, \tag{2.48}$$

$$\frac{\partial C_l}{\partial \tau} + \frac{\partial}{\partial Y} \left(C_l \hat{U} \right) = 0. \tag{2.49}$$

Note, incidentally, that there is no trace of any terms involving the reference temperature in equations (2.44) and (2.48), as these vanish as a consequence of (2.43) and (2.47) and the fact that we have taken $c_{ps} = c_{pl}$.

The boundary and interfacial conditions are then, at $Y = 0$,

$$\theta = 0; \tag{2.50}$$

at $Y = Y_s(\tau)$,

$$\begin{cases} \chi = 0, \quad \theta = \theta_m - \tilde{m} C_l, & \text{if } C_l < C_{eut}, \\ \theta = \theta_{eut}, & \text{if } C_l = C_{eut}, \end{cases} \tag{2.51}$$

$$\left[\frac{\partial \theta}{\partial Y} \right]_-^+ = -\frac{\chi_s}{St} \dot{Y}_s(\tau), \tag{2.52}$$

$$\hat{U} = (1 - R) \chi_s \dot{Y}_s(\tau), \tag{2.53}$$

https://doi.org/10.1017/S0956792520000091 Published online by Cambridge University Press

where

$$\theta_{\text{eut}} = \frac{T_{\text{eut}} - T_{\text{w}}}{T_{\text{cast}} - T_{\text{w}}};$$

at $Y = Y_{\text{l}}(\tau)$,

$$\theta = \theta_{\text{m}} - \tilde{m} C_{\text{l}}, \tag{2.54}$$

$$\left[\frac{\partial \theta}{\partial Y}\right]_{-}^{+} = 0, \tag{2.55}$$

$$\chi = 1; \tag{2.56}$$

at $Y = Y_{\infty}(\tau)$,

$$\frac{\partial \theta}{\partial Y} = 0, \tag{2.57}$$

$$\frac{\partial C_{\text{l}}}{\partial Y} = 0. \tag{2.58}$$

As for the initial conditions, we have, for $0 < Y \leqslant 1$,

$$\theta = 1, \tag{2.59}$$

$$C_{\text{l}} = C_0, \tag{2.60}$$

as well as

$$Y_{\text{l}}(0) = 0, \tag{2.61}$$

$$Y_{\text{s}}(0) = 0, \tag{2.62}$$

$$Y_{\infty}(0) = 1. \tag{2.63}$$

Also, from (2.40), we have

$$\int_0^{Y_{\infty}(\tau)} \rho C \mathrm{d}Y = \rho_{\text{l}} C_0. \tag{2.64}$$

3 Analysis

3.1 Transformed equations

As already mentioned, we cannot expect a similarity solution for general τ and, rather than expecting to be able to proceed in terms of the usual $Y/\tau^{1/2}$ similarity variable, we introduce a triple Landau transformation, with a view to posing the problem on a fixed spatial domain, via

$$\eta = \begin{cases} Y/Y_{\text{s}}(\tau), & 0 < Y < Y_{\text{s}}(\tau) \\ 1 + \dfrac{Y - Y_{\text{s}}(\tau)}{Y_{\text{l}}(\tau) - Y_{\text{s}}(\tau)}, & Y_{\text{s}}(\tau) < Y < Y_{\text{l}}(\tau) \\ 2 + \dfrac{Y - Y_{\text{l}}(\tau)}{Y_{\infty}(\tau) - Y_{\text{l}}(\tau)}, & Y_{\text{l}}(\tau) < Y < Y_{\infty}(\tau) \end{cases} \tag{3.1}$$

https://doi.org/10.1017/S0956792520000091 Published online by Cambridge University Press

and

$$\theta = F(\eta, \tau), \quad \hat{U} = \tau^{-1/2}\tilde{U}(\eta, \tau), \quad \chi = \chi(\eta, \tau), \quad C_l = C_l(\eta, \tau); \tag{3.2}$$

although transformation (3.1) may appear to complicate the subsequent algebra, it makes the behaviour of the governing equations in the limit as $\tau \to 0$ more transparent. Of note here is the supposition that $\hat{U}$ will behave as $\tau^{-1/2}$ as $\tau \to 0$; however, this is exactly the behaviour that was assumed in [31], and we will find here also that it leads to a sensibly posed problem for $\tilde{U}$. Furthermore, it is the behaviour seen in the classical two-phase Neumann problem when the solid and liquid densities are different [1, 7] and is merely a natural consequence of the velocity of the solidification front itself behaving initially as $\tau^{-1/2}$, even when the solid and liquid densities are equal.

We will have, for $0 \leqslant \eta \leqslant 1$,

$$R\left(Y_s^2\frac{\partial F}{\partial \tau} - \eta Y_s \dot{Y}_s \frac{\partial F}{\partial \eta}\right) = \frac{\partial^2 F}{\partial \eta^2}; \tag{3.3}$$

for $1 \leqslant \eta \leqslant 2$,

$$(1-R)\left(\frac{\partial \chi}{\partial \tau} + \eta_\tau \frac{\partial \chi}{\partial \eta}\right) + \frac{1}{\tau^{1/2}(Y_l(\tau) - Y_s(\tau))}\frac{\partial \tilde{U}}{\partial \eta} = 0, \tag{3.4}$$

$$[\chi + (1-\chi)R]\left(\frac{\partial F}{\partial \tau} + \eta_\tau \frac{\partial F}{\partial \eta}\right) + \frac{\tilde{U}}{\tau^{1/2}(Y_l(\tau) - Y_s(\tau))}\frac{\partial F}{\partial \eta}$$

$$= \frac{1}{(Y_l(\tau) - Y_s(\tau))^2}\frac{\partial^2 F}{\partial \eta^2} - \frac{R}{St}\left(\frac{\partial \chi}{\partial \tau} + \eta_\tau \frac{\partial \chi}{\partial \eta}\right), \tag{3.5}$$

$$\frac{\partial}{\partial \tau}(\chi C_l) + \eta_\tau \frac{\partial}{\partial \eta}(\chi C_l) - k_0 R C_l\left(\frac{\partial \chi}{\partial \tau} + \eta_\tau \frac{\partial \chi}{\partial \eta}\right) + \beta R(1-\chi)k_0\left(\frac{\partial C_l}{\partial \tau} + \eta_\tau \frac{\partial C_l}{\partial \eta}\right)$$

$$+ \frac{1}{\tau^{1/2}(Y_l(\tau) - Y_s(\tau))}\frac{\partial}{\partial \eta}\left(C_l \tilde{U}\right) = 0, \tag{3.6}$$

$$F = \theta_m - \tilde{m} C_l, \tag{3.7}$$

where

$$\eta_\tau = -\left\{\frac{\dot{Y}_s(\tau) + (\eta - 1)\left(\dot{Y}_l(\tau) - \dot{Y}_s(\tau)\right)}{(Y_l(\tau) - Y_s(\tau))}\right\},$$

with dots denoting differentiation with respect to τ, for $2 \leqslant \eta < 3$,

$$\frac{\partial \tilde{U}}{\partial \eta} = 0, \tag{3.8}$$

https://doi.org/10.1017/S0956792520000091 Published online by Cambridge University Press

$$(Y_\infty(\tau)-Y_1(\tau))^2\frac{\partial F}{\partial \tau}-\left\{\dot{Y}_1(\tau)+(\eta-2)\left(\dot{Y}_\infty(\tau)-\dot{Y}_1(\tau)\right)\right\}(Y_\infty(\tau)-Y_1(\tau))\frac{\partial F}{\partial \eta}$$
$$+\frac{(Y_\infty(\tau)-Y_1(\tau))}{\tau^{1/2}}\tilde{U}\frac{\partial F}{\partial \eta}=\frac{\partial^2 F}{\partial \eta^2}, \tag{3.9}$$

$$(Y_\infty(\tau)-Y_1(\tau))\frac{\partial C_1}{\partial \tau}+\left(\frac{\tilde{U}}{\tau^{1/2}}-\left\{\dot{Y}_1(\tau)+(\eta-2)\left(\dot{Y}_\infty(\tau)-\dot{Y}_1(\tau)\right)\right\}\right)\frac{\partial C_1}{\partial \eta}=0. \tag{3.10}$$

The boundary conditions are, at $\eta=0$,

$$F=0; \tag{3.11}$$

at $\eta=1$,

$$\begin{cases}\chi=0, \quad F=\theta_m-\tilde{m}C_1, & \text{if } C_1<C_{eut},\\ F=\theta_{eut}, & \text{if } C_1=C_{eut},\end{cases} \tag{3.12}$$

$$\frac{1}{Y_1(\tau)-Y_s(\tau)}\left(\frac{\partial F}{\partial \eta}\right)_+-\frac{1}{Y_s(\tau)}\left(\frac{\partial F}{\partial \eta}\right)_-=-\frac{\chi_s}{St}\dot{Y}_s(\tau), \tag{3.13}$$

$$\tilde{U}=(1-R)\,\chi_s\tau^{1/2}\dot{Y}_s(\tau); \tag{3.14}$$

at $\eta=2$,

$$F=\theta_m-\tilde{m}C_1, \tag{3.15}$$

$$\frac{1}{Y_\infty(\tau)-Y_1(\tau)}\left(\frac{\partial F}{\partial \eta}\right)_+-\frac{1}{Y_1(\tau)-Y_s(\tau)}\left(\frac{\partial F}{\partial \eta}\right)_-=0, \tag{3.16}$$

$$\chi=1; \tag{3.17}$$

at $\eta=3$,

$$\frac{\partial F}{\partial \eta}=0, \tag{3.18}$$

$$\frac{\partial C_1}{\partial \eta}=0. \tag{3.19}$$

As for the initial conditions, we have, for $0<\eta\leqslant 3$,

$$F=1, \tag{3.20}$$

$$C_1=C_0, \tag{3.21}$$

as well as

$$Y_1(0)=0, \tag{3.22}$$

$$Y_s(0)=0, \tag{3.23}$$

$$Y_\infty(0)=1. \tag{3.24}$$

https://doi.org/10.1017/S0956792520000091 Published online by Cambridge University Press

3.2 The limit as $\tau \to 0$

We must now consider these equations in the limit as $\tau \to 0$. We will have that $Y_l, Y_s \to 0$ as $\tau \to 0$, and it is plausible to suppose that $Y_l, Y_s \sim \tau^{1/2}$; we will therefore set

$$Y_l \sim \eta_{liq}\tau^{1/2}, \quad Y_s \sim \eta_{sol}\tau^{1/2},$$

where η_{liq} and η_{sol} are to be determined. Previous experience in the solution of Stefan problems for which the domain of interest initially has zero thickness [23–25] indicates that, as $\tau \to 0$, we should just obtain a system of ODEs. In this case, with primes denoting differentiation with respect to η, we arrive at, for $0 \leqslant \eta \leqslant 1$,

$$-\frac{1}{2}R\eta_{sol}^2\eta F' = F''; \tag{3.25}$$

for $1 \leqslant \eta \leqslant 2$,

$$-\frac{1}{2}(1-R)\left\{(2-\eta)\,\eta_{sol} + (\eta-1)\,\eta_{liq}\right\}\chi' + \tilde{U}' = 0, \tag{3.26}$$

$$\left(\eta_{liq}-\eta_{sol}\right)\left[\tilde{U} - \frac{1}{2}\left[\chi + (1-\chi)\,R\right]\left\{(2-\eta)\,\eta_{sol} + (\eta-1)\,\eta_{liq}\right\}\right]F'$$

$$= F'' + \frac{1}{2}\frac{R}{St}\left(\eta_{liq}-\eta_{sol}\right)\left\{(2-\eta)\,\eta_{sol} + (\eta-1)\,\eta_{liq}\right\}\chi', \tag{3.27}$$

$$\frac{1}{2}\left\{(2-\eta)\,\eta_{sol} + (\eta-1)\,\eta_{liq}\right\}\left[k_0RC_l\chi' - (\chi C_l)' - \beta R\,(1-\chi)\,k_0C_l'\right] + \left(C_l\tilde{U}\right)' = 0 \tag{3.28}$$

$$F = \theta_m - \tilde{m}C_l; \tag{3.29}$$

for $2 \leqslant \eta < 3$,

$$\tilde{U}' = 0, \tag{3.30}$$

$$F' = 0, \tag{3.31}$$

$$C_l' = 0. \tag{3.32}$$

The boundary conditions are, at $\eta = 0$,

$$F = 0; \tag{3.33}$$

at $\eta = 1$,

$$\begin{cases} \chi = 0, \quad F = \theta_m - \tilde{m}C_l, & \text{if } C_l < C_{eut}, \\ F = \theta_{eut}, & \text{if } C_l = C_{eut}, \end{cases} \tag{3.34}$$

$$\frac{(F')_+}{\eta_{liq}-\eta_{sol}} - \frac{(F')_-}{\eta_{sol}} = -\frac{\chi_s\eta_{sol}}{2St}, \tag{3.35}$$

$$\tilde{U} = \frac{1}{2}(1-R)\,\chi_s\eta_{sol}; \tag{3.36}$$

https://doi.org/10.1017/S0956792520000091 Published online by Cambridge University Press

at $\eta = 2$,

$$F = \theta_{\mathrm{m}} - \tilde{m} C_{\mathrm{l}}, \tag{3.37}$$

$$\left(F'\right)_{-} = 0, \tag{3.38}$$

$$\chi = 1; \tag{3.39}$$

at $\eta = 3$,

$$F' = 0, \tag{3.40}$$

$$C_{\mathrm{l}}' = 0. \tag{3.41}$$

There is now clearly a problem for $2 \leqslant \eta \leqslant 3$ since (3.31), subject to (3.20) and (3.40), implies that $F \equiv 1$, which contradicts (3.37). This is not surprising, since the second derivative in η in (3.9) was neglected; in order for it to be retained, we would need a boundary layer for which $\eta - 2 \sim \tau^{1/2}$, and so we need a further transformation,

$$\hat{\eta} = \frac{\eta - 2}{\tau^{1/2}}, \quad \mathcal{F} = F, \tag{3.42}$$

so that (3.9) becomes

$$\left(Y_{\infty}(\tau) - Y_{\mathrm{l}}(\tau)\right)^2 \left(\tau \frac{\partial \mathcal{F}}{\partial \tau} - \frac{1}{2}\hat{\eta} \frac{\partial \mathcal{F}}{\partial \hat{\eta}}\right)$$

$$+ \left\{\tilde{U} - \tau^{1/2}\left\{\dot{Y}_{\mathrm{l}}(\tau) + \hat{\eta}\tau^{1/2}\left(\dot{Y}_{\infty}(\tau) - \dot{Y}_{\mathrm{l}}(\tau)\right)\right\}\right\}\left(Y_{\infty}(\tau) - Y_{\mathrm{l}}(\tau)\right) \frac{\partial \mathcal{F}}{\partial \hat{\eta}} = \frac{\partial^2 \mathcal{F}}{\partial \hat{\eta}^2}, \tag{3.43}$$

leading to, as $\tau \to 0$,

$$Y_{\infty}(0)\left(\tilde{U} - \frac{1}{2} Y_{\infty}(0)\,\hat{\eta} - \frac{1}{2}\eta_{\mathrm{liq}}\right) \frac{\mathrm{d}\mathcal{F}}{\mathrm{d}\hat{\eta}} = \frac{\mathrm{d}^2 \mathcal{F}}{\mathrm{d}\hat{\eta}^2}, \tag{3.44}$$

where $\mathcal{F}$ satisfies

$$\mathcal{F} = \theta_{\mathrm{m}} - \tilde{m} C_{\mathrm{l}} \quad \text{at } \hat{\eta} = 0, \tag{3.45}$$

$$\mathcal{F} \to 1 \quad \text{as } \hat{\eta} \to \infty. \tag{3.46}$$

Also, (3.16) now becomes, instead of (3.38),

$$\frac{\left(\mathcal{F}'\right)_{\hat{\eta}=0}}{Y_{\infty}(0)} = \frac{\left(F'\right)_{\eta=2_-}}{\eta_{\mathrm{liq}} - \eta_{\mathrm{sol}}}. \tag{3.47}$$

For $0 \leqslant \eta \leqslant 1$, there is an analytical solution in the form

$$F = \frac{\theta_{\mathrm{s}} \operatorname{erf}\left(\frac{R^{1/2}\eta}{2}\right)}{\operatorname{erf}\left(\frac{R^{1/2}\eta_{\mathrm{sol}}}{2}\right)}, \tag{3.48}$$

where $\theta_{\mathrm{s}} = (F)_{\eta=1}$; thus, θ_{s} must itself be iterated for via (3.34). To obtain the solution to (3.44)–(3.46), we set

$$\bar{\eta} = \left(Y_{\infty}(0)\,\hat{\eta} + \eta_{\mathrm{liq}} - 2\tilde{U}\right) / Y_{\infty}^{1/2}(0), \tag{3.49}$$

https://doi.org/10.1017/S0956792520000091 Published online by Cambridge University Press

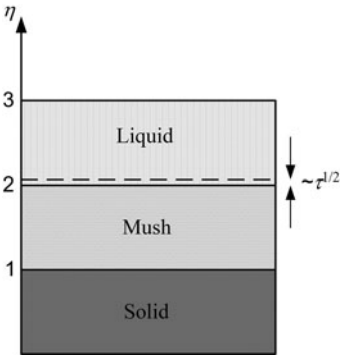


FIGURE 3. Schematic of the solution structure for small τ in the η-space. The dashed line indicates a boundary layer in θ of width $\tau^{1/2}$, with $\eta - 2 \sim \tau^{1/2}$.

leading to

$$-\frac{1}{2}\bar{\eta}\mathcal{F}' = \mathcal{F}'', \tag{3.50}$$

subject to

$$\mathcal{F} = \theta_{\mathrm{m}} - \tilde{m}C_{\mathrm{l}} \quad \text{at } \bar{\eta} = \left(\eta_{\mathrm{liq}} - 2\tilde{U}\right)/Y_{\infty}^{1/2}(0)\,, \tag{3.51}$$

$$\mathcal{F} \to 1 \quad \text{as } \bar{\eta} \to \infty. \tag{3.52}$$

Now,

$$\mathcal{F} = A\,\mathrm{erf}\left(\frac{\bar{\eta}}{2}\right) + B, \tag{3.53}$$

where

$$A = \frac{1 - \theta_{\mathrm{liq}}}{1 - \mathrm{erf}\left(\frac{\eta_{\mathrm{liq}} - 2\tilde{U}}{2Y_{\infty}^{1/2}(0)}\right)}, \quad B = \frac{\theta_{\mathrm{liq}} - \mathrm{erf}\left(\frac{\eta_{\mathrm{liq}} - 2\tilde{U}}{2Y_{\infty}^{1/2}(0)}\right)}{1 - \mathrm{erf}\left(\frac{\eta_{\mathrm{liq}} - 2\tilde{U}}{2Y_{\infty}^{1/2}(0)}\right)}, \tag{3.54}$$

where $\theta_{\mathrm{liq}} = \theta_{\mathrm{m}} - \tilde{m}C_0$. Note that the latter comes from (3.32) and (3.41), which both imply that $C_{\mathrm{l}} = C_0$ at $\eta = 2$; also, observe that, although there is a boundary layer for F at $\eta = 2$ as $\tau \to 0$, there is no boundary layer for C_{l}.

A schematic of the solution structure for small τ in the η-space is given in Figure 3, showing the aforementioned boundary layer. Moreover, it appears that such a boundary layer would also be present in the problem of a solidifying sphere that was considered in [21]; the corresponding analysis to demonstrate this is given in Appendix B.

4 Results

Here, we first focus, in Section 4.1, on analytical results that can be extracted when $R = 1$, before moving on to give solutions for $R \neq 1$ in Section 4.2; the focus here is on the similarity solution for small times. In addition, in Appendix C, we compare our results with those in [31].

https://doi.org/10.1017/S0956792520000091 Published online by Cambridge University Press

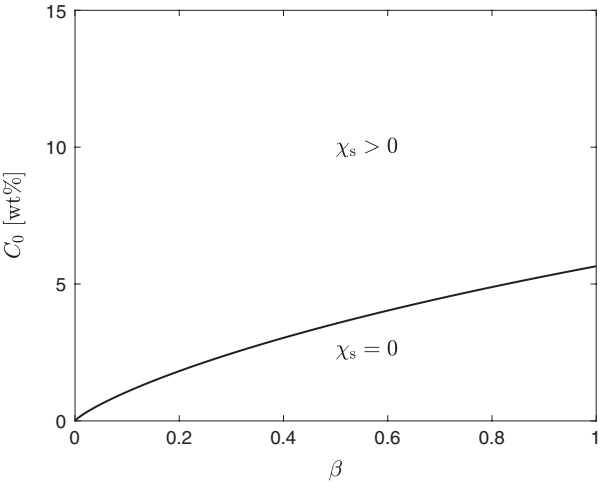


FIGURE 4. The curve in (β, C_0)-space which determines whether $\chi_s = 0$ or $\chi_s > 0$ $(R = 1)$.

4.1 $R = 1$

In this case, equation (2.45), with the assistance of (2.43), reduces to

$$\frac{\partial}{\partial \tau}(\chi C_l) - k_0 C_l \frac{\partial \chi}{\partial \tau} + \beta (1 - \chi) k_0 \frac{\partial C_l}{\partial \tau} = 0; \tag{4.1}$$

this can be integrated exactly to give, on using the fact that $C_l = C_0$ when $\chi = 1$,

$$C_l = C_0 (\chi + \beta k_0 (1 - \chi))^{\frac{k_0 - 1}{1 - \beta k_0}}. \tag{4.2}$$

The next question concerns what should be the value of χ_s, that is, χ at $Y = Y_s(\tau)$. For example, if $\chi_s = 0$, we must have

$$C_l = C_0 (\beta k_0)^{\frac{k_0 - 1}{1 - \beta k_0}}$$

there, and we therefore would need

$$C_0 (\beta k_0)^{\frac{k_0 - 1}{1 - \beta k_0}} < C_{\text{eut}}; \tag{4.3}$$

otherwise, we have $\chi_s > 0$. An expression for χ_s valid for both cases is then

$$\chi_s = \max\left(0, \frac{1}{1 - \beta k_0}\left\{\left(\frac{C_0}{C_{\text{eut}}}\right)^{\frac{1 - \beta k_0}{1 - k_0}} - \beta k_0\right\}\right). \tag{4.4}$$

Figure 4 shows the curve in (β, C_0)-space, based on (4.3), which delineates whether $\chi_s = 0$ or $\chi_s > 0$; thus, as β decreases, the range of values of C_0 for which eutectic solidification occurs, that is, $\chi_s > 0$, increases. On the other hand, Figure 5 shows χ_s as a function of β, as given in equation (4.4), for three different values of C_0. Of significance here is the fact that $\chi_s = 0$ for $\beta \gtrsim 0.8$ for the lowest value of C_0 given; hence, for values of β lower than this, eutectic solidification would occur. Moreover, for eutectic solidification to occur for the whole range

https://doi.org/10.1017/S0956792520000091 Published online by Cambridge University Press

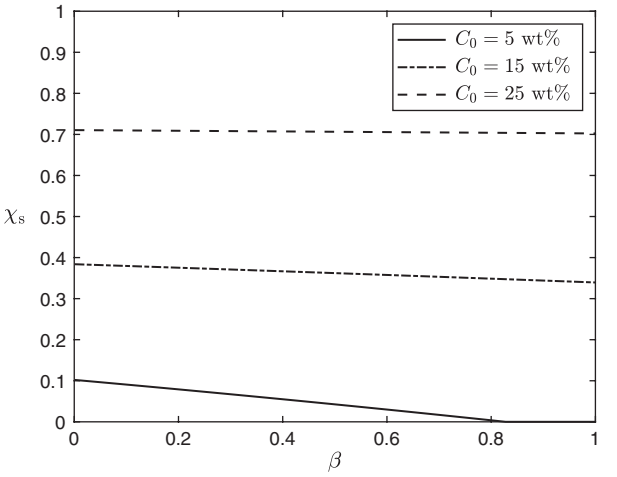


FIGURE 5. χ_s as a function of β for three values of C_0 ($R = 1$).

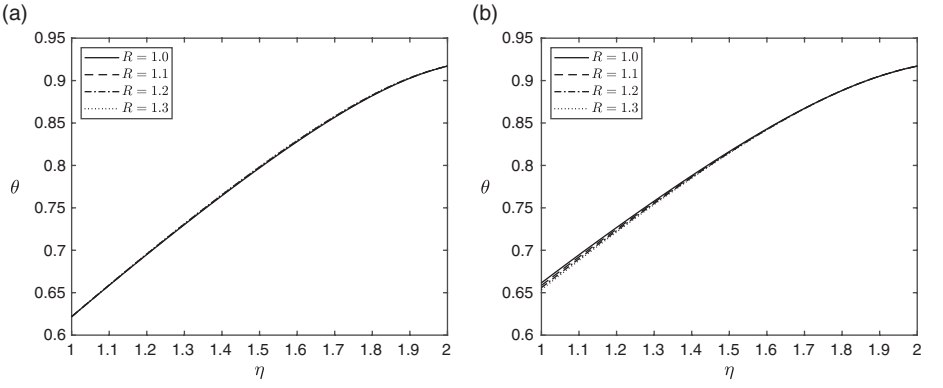


FIGURE 6. θ as a function of η for four values of R for (a) $\beta = 0$ and (b) $\beta = 1$.

of β, we would need $k_0 C_{\text{eut}} < C_0 \leqslant C_{\text{eut}}$, as would be obtained by requiring $\chi_s > 0$ for $\beta = 1$ in equation (4.4).

4.2 $R \neq 1$

In this case, we do not have equation (4.2) for guidance, and consequently there is no closed-form expression for χ_s, which must instead be computed numerically as part of the solution; neither do we know at what value of β the transition from non-eutectic to eutectic solidification would occur. In what follows, we therefore consider first just small τ – in fact, in the limit as $\tau \to 0$ – and indicate later how the treatment would differ for $\tau > 0$.

Results are given below for $C_0 = 5$ wt% Cu and $R = 1, 1.1, 1.2, 1.3$; the value of C_0 is the same as that used in [31], although a key difference is that these results are only for the limit as $\tau \to 0$ and would be different for $\tau > 0$, that is, there is no similarity solution that is valid for all time.

Figure 6(a) and (b) shows θ as a function of η ($1 \leqslant \eta \leqslant 2$) for four values of R when $\beta = 0$ and $\beta = 1$, respectively. The curves in Figure 6(a) appear to lie on top of each other, which is

https://doi.org/10.1017/S0956792520000091 Published online by Cambridge University Press

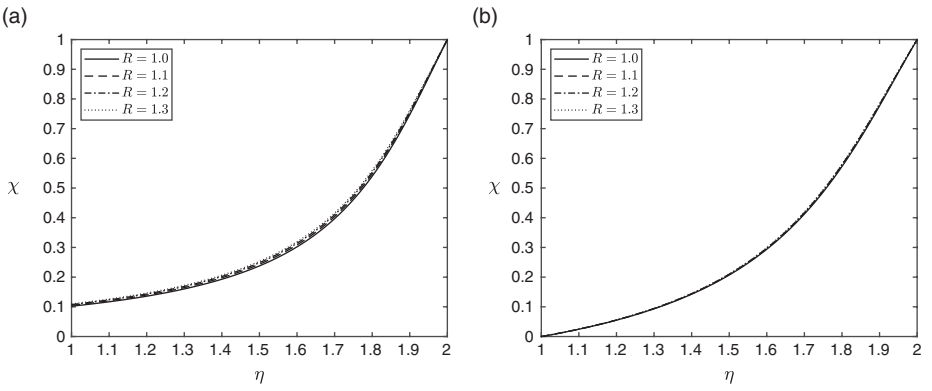


FIGURE 7. χ as a function of η for four values of R for (a) $\beta = 0$ and (b) $\beta = 1$.

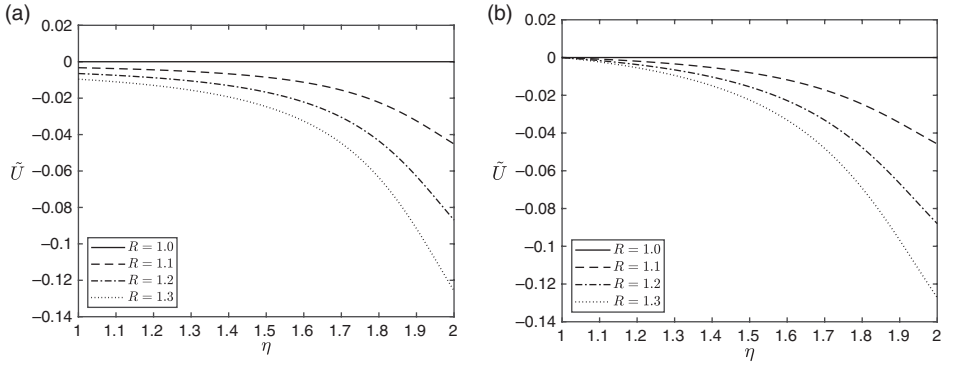


FIGURE 8. $\tilde{U}$ as a function of η for four values of R for (a) $\beta = 0$ and (b) $\beta = 1$.

a consequence of the fact that $\theta = \theta_{\text{eut}}$ at $\eta = 1$ and $\theta = \theta_{\text{m}} - \tilde{m}C_0$ at $\eta = 2$ for all of them. In Figure 6(b), on the other hand, $\theta > \theta_{\text{eut}}$ at $\eta = 1$, and there is some variation, with θ at $\eta = 1$ decreasing as R increases.

Figure 7(a) and (b) shows χ as a function of η for the same four values of R when $\beta = 0$ and $\beta = 1$, respectively. In both plots, the value of χ at $\eta = 1$ for $R = 1$ corresponds to the values for χ_{s} shown in Figure 5; however, for $\beta = 0$, the value of χ_{s} increases with R, but remains zero for $\beta = 1$, indicating that $C_{\text{l}} < C_{\text{eut}}$ for all four curves in this plot.

Figure 8(a) and (b) shows $\tilde{U}$ as a function of η for four values of R when $\beta = 0$ and $\beta = 1$, respectively. Here, the profiles change significantly with respect to R, although less so with respect to β. In particular, the values of $\tilde{U}$ at $\eta = 2$ are almost identical for $\beta = 0$ and $\beta = 1$, but are equal to zero at $\eta = 1$ for the latter; this is because $\chi_{\text{s}} = 0$.

Figure 9(a) and (b) shows η_{sol} and η_{liq} as functions of β for the same four values of R. Most distinct here are the kinks in Figure 9(a) for β just in excess of 0.8. Whereas these might be expected for the $R = 1$ curves, in view of the earlier discussion in Section 4.1, the kinks for the other curves indicate that a similar transition from non-eutectic to eutectic solidification occurs; in fact, further computations for more values of β in the interval $0.8 \leqslant \beta \leqslant 0.85$ indicated that the critical value of β for the transition increased as R was increased. On the other hand, no kinks

https://doi.org/10.1017/S0956792520000091 Published online by Cambridge University Press

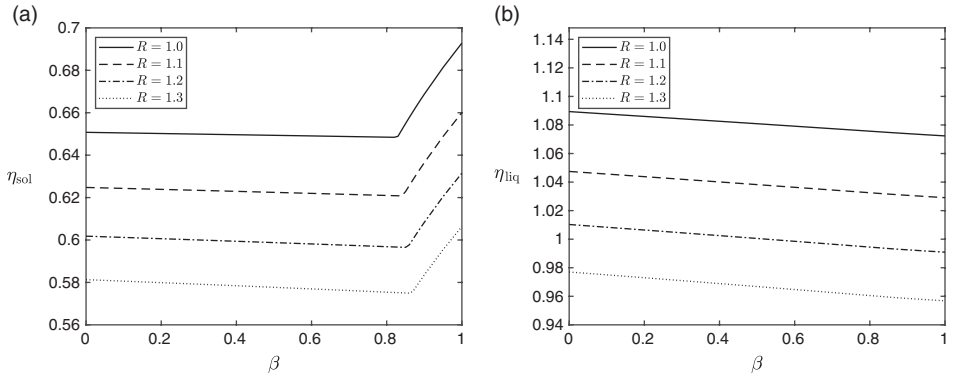


FIGURE 9. $\eta_{\rm sol}$ (a) and $\eta_{\rm liq}$ (b) as functions of β for four values of R.

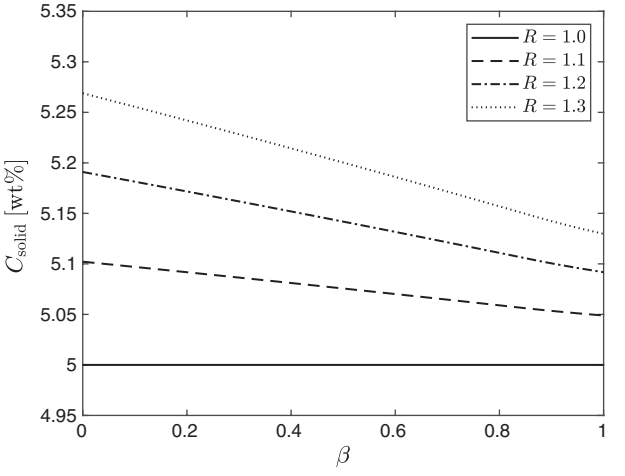


FIGURE 10. The solute concentration in the solid, $C_{\rm solid}$, as a function of β for four values of R.

are visible in Figure 9(b) although, most likely, it is the case that the kinks are extremely mild in this case – a reflection of the fact that their cause is at the solidus boundary, rather than at the liquid boundary.

Finally, we note that although we have so far computed only in the limit as $\tau \to 0$, we can nevertheless demonstrate the well-known phenomenon of inverse segregation, whereby the solute concentration is higher at the cooling surface. Figure 10 shows the solute concentration in the fully solidified region, which we shall denote by $C_{\rm solid}$, as a function of β for four values of R; note that in general $C_{\rm solid} \neq C_{\rm s}|_{\eta=1}$, but must be computed from (2.12) as

$$\rho_{\rm s} C_{\rm solid} = \chi_{\rm s}\rho_{\rm l}\ C_{\rm l}|_{\eta=1} + \rho_{\rm s}\int_0^{1-\chi_{\rm s}} \left(C_{\rm s} + \beta\chi'\frac{{\rm d}C_{\rm s}}{{\rm d}\chi'}\right){\rm d}\chi'. \tag{4.5}$$

From the figure, it is evident that $C_{\rm solid} > C_0$ for $R > 1$, but that $C_{\rm solid} = C_0$ for $R = 1$, as would be expected; in addition, kinks are just about visible in the curves for which $R > 1$, for the reasons discussed in the previous paragraph, although these are much milder than in Figure 9(a).

https://doi.org/10.1017/S0956792520000091 Published online by Cambridge University Press

5 Conclusions

In this paper, we have considered the one-dimensional solidification of a binary alloy undergoing shrinkage; this is arguably the simplest possible configuration for the occurrence of macrosegregation and therefore constitutes an invaluable benchmark for the testing of numerical codes that model these phenomena. We have extended an earlier obtained solution for this problem [31], that was posed on a semi-infinite spatial domain and valid for the case of low superheat and eutectic solidification, to the more general situation of a finite spatial domain, arbitrarily large superheat and both eutectic and non-eutectic solidification. In so doing, we found that a similarity solution is available only for short times, and that this contains a boundary layer on the liquid side of the mush–liquid interface. Note that this boundary layer seems somewhat unexpected, since the usual reason for the appearance of a boundary layer – namely, a small dimensionless parameter multiplying the highest order derivative in a differential equation, as occurred in [21] for large Stefan number – does not occur; instead, it seems only to have become prominent because of a series of transformations that were essential for considering the small-time behaviour of the problem. Moreover, we believe that this small-time solution constitutes the correct initial condition for the subsequent numerical solution of the full non-similar problem. Whilst this can only be definitively shown for this problem by providing a numerical solution to the system of partial differential equations (PDEs), a task that is deferred to future work, we note the reasons why we believe that this will be the case. The procedure that we have adopted, that is, formulating a system of PDEs which becomes degenerate as $t \to 0$ when there is no solid or mush, thereby requiring a self-starting similarity solution, is analogous to that which we have used with success in a number of similar, albeit slightly simpler, solidification problems that have involved both a pure material, having a distinct phase-change temperature [23–25], and alloys having solidus and liquidus temperatures [38, 39]. Admittedly, however, none of these problems involved a square-root singularity in the velocity, but the fact that we have shown a self-consistent reduction of the full PDEs to ODEs in the limit as $t \to 0$, in a manner analogous to that in [23–25, 38, 39], is a positive sign.

Mathematically, the problem is similar to that of macrosegregation in steady-state continuous casting treated recently by [39]. On the one hand, the current problem is simpler, since the solid and mushy regions are both initiated at time $t = 0$. However, [39] treated the problem as a regular perturbation in the small parameter $(\rho_s/\rho_l - 1)$, considered only the case $\beta = 1$ and assumed zero superheat, that is, $T_{cast} = T_{liq}$, whereas the present treatment does not depend on any of these assumptions. Also, although this paper has not provided the analysis for the case when $C_0 = C_{eut}$, this is considerably easier than for when $C_0 < C_{eut}$, since it is only necessary to consider the solid and melt, as no mushy region is present; hence, only the temperature needs to be solved for. Indeed, a similarity solution for this case has been provided previously [1, 7, 11]. A further comment concerns the link between similarity solutions and macrosegregation. It was suggested in [31] that the use of a constant cooling temperature leads to a constant level for macrosegregation even when $R \neq 1$; this was because of the similarity solution adopted there. On the other hand, the results given by us, even although only so far in the limit as $t \to 0$, indicate that the constant temperature condition will lead to inverse segregation, as mentioned earlier.

The wider significance of the results given here is that they may provide the correct initial conditions for solving the complete problem, that is, for the solidification of the entire melt. In particular, they appear to give a framework for solving the problem using a moving mesh

https://doi.org/10.1017/S0956792520000091 Published online by Cambridge University Press

formulation, rather than the more commonly used enthalpy formulation, which employs a fixed mesh. As a consequence, this avoids the need to use artificial parameters to ensure numerical convergence [2, 3]; this is because the governing equations are far from the usual advection-diffusion form that is suitable for computational fluid dynamics, but consist of a diffusionless transport equation (2.7) and an algebraic relation (2.13). In addition, this approach would be well suited not just to problems involving two moving boundaries, but also when the boundaries are not planar, as was demonstrated in [36,37] for the two-dimensional problem of the solidification of one-component material in the presence of natural convection in an enclosure. By tracking the solidus and liquid interfaces explicitly, it is hoped to be able to avoid the usual issues of numerical dispersion and diffusion that are present in the numerically simulated macrosegregation profiles reported in the literature [15,34,35].

Acknowledgements

The authors would also like to thank the anonymous reviewers for their important comments and suggestions.

Conflicts of interest

None.

References

[1] Alexiades, V. & Solomon, A. D. (1993) *Mathematical Modelling of Melting and Freezing Processes*, Hemisphere Publishing Corporation, Washington, DC.
[2] Amberg, G. (1991) Computation of macrosegregation in an iron-carbon cast. *Int. J. Heat Mass Transfer* **34**, 217–227.
[3] Assunção, M. & Vynnycky, M. (2018) Mathematical modelling of macrosegregation in ingot casting. *Engenharia Térmica (Therm. Eng.)* **17**(2), 74–79.
[4] Bennon, W. D. & Incropera, F. P. (1987) A continuum model for momentum, heat and species transport in binary solid-liquid phase change systems – I. Model formulation. *Int. J. Heat Mass Transfer* **30**(10), 2161–2170.
[5] Brody, H. B. & Flemings, M. C. (1966) Solute redistribution in dendritic solidification. *Trans. AIME* **236**(12), 615–624.
[6] Brosa Planella, F., Please, C. P. & Van Gorder, R. A. (2019) Extended Stefan problem for solidification of binary alloys in a finite planar domain. *SIAM J. Appl. Math.* **79**, 876–913.
[7] Carslaw, H. S. & Jaeger, J. C. (1959) *Conduction of Heat in Solids*, 2nd ed., Oxford University Press, Oxford.
[8] Chakraborty, S. & Dutta, P. (2002) An analytical solution for conduction-dominated unidirectional solidification of binary mixtures. *Appl. Math. Mod.* **26**, 545–561.
[9] Chen, J. H. & Tsai, H. L. (1993) Inverse segregation for a unidirectional solidification of aluminium-copper alloys. *Int. J. Heat Mass Transfer* **36**, 3069–3075.
[10] Clyne, T. W. & Kurz, W. (1981) Solute redistribution during solidification with rapid solid-state diffusion. *Met. Trans. A* **12**(6), 965–971.
[11] Crank, J. (1984) *Free and Moving Boundary Problems*, Clarendon Press, Oxford.
[12] Davis, G. B. & Hill, J. M. (1982) A moving boundary problem for the sphere. *IMA J. Appl. Math.* **29**, 99–111.
[13] Diao, Q. Z. & Tsai, H. L. (1993) Modelling of solute redistribution in the mushy zone during solidification of aluminium-copper alloys. *Metall. Trans.* **24A**, 963–973.

https://doi.org/10.1017/S0956792520000091 Published online by Cambridge University Press

[14] DIAO, Q. Z. & TSAI, H. L. (1993) The formation of negative- and positive-segregated bands during solidification of aluminum-copper alloys. *Int. J. Heat Mass Transfer* **36**, 4299–4305.
[15] DU, Q., ESKIN, D. G. & KATGERMAN, L. (2009) Numerical issues in modelling macrosegregation during DC casting of a multi-component aluminium alloy. *Int. J. Num. Meth. Heat Fluid Flow* **19**, 910–930.
[16] FELTHAM, D. L. & GARSIDE, J. (2001) Analytical and numerical solutions describing the inward solidification of a binary melt. *Chem. Eng. Sci.* **56**, 2357–2370.
[17] FLEMINGS, M. C. (1974) *Solidification Processing*, McGraw-Hill, New York, NY.
[18] JAKHAR, A., RATH, P. & MAHAPATRA, S. K. (2016) A similarity solution for phase change of binary alloy with shrinkage or expansion. *Eng. Sci. Technol - Int. J. - JESTECH* **19**, 1390–1399.
[19] JALANTI, T., SWIERKOSZ, M., GREMAUD, M. & RAPPAZ, M. (2006) Modelling of macrosegregation in continuous casting of aluminium. In: K. Ehrke and W. Schneider (editors), *Continuous Casting*, WILEY-VCH Verlag GmbH, Weinheim, pp. 191–198.
[20] KUCERA, A. & HILL, J. M. (1986) On inward solidifying cylinders and spheres initially not at their fusion temperature. *Int. J. Nonlinear Mech.* **21**, 73–82.
[21] MCCUE, S. W., BISHENG, W. & HILL, J. M. (2008) Classical two-phase Stefan problem for spheres. *Proc. R. Soc. A* **464**, 2055–2076.
[22] MINAKAWA, S., SAMARASEKERA, I. V. & WEINBERG, F. (1985) Inverse segregation. *Metall. Trans.* **16B**, 595–604.
[23] MITCHELL, S. L. & VYNNYCKY, M. (2009) Finite-difference methods with increased accuracy and correct initialization for one-dimensional Stefan problems. *Appl. Math. Comp.* **215**, 1609–1621.
[24] MITCHELL, S. L. & VYNNYCKY, M. (2014) On the numerical solution of two-phase Stefan problems with heat-flux boundary conditions. *J. Comp. Appl. Math.* **264**, 49–64.
[25] MITCHELL, S. L. & VYNNYCKY, M. (2016) On the accurate numerical solution of a two-phase Stefan problem with phase formation and depletion. *J. Comp. Appl. Math.* **300**, 259–274.
[26] MO, A. (1993) Mathematical modelling of surface segregation in aluminum DC casting caused by exudation. *Int. J. Heat Mass Transfer* **36**, 4335–4340.
[27] MULLINS, W. W. & SEKERKA, R. F. (1964) Stability of a planar interface during solidification of a dilute binary alloy. *J. Appl. Phys.* **35**, 444–451.
[28] SWAMINATHAN, C. R. & VOLLER, V. R. (1997) Towards a general numerical scheme for solidification systems. *Int. J. Heat Mass Transfer* **40**, 2859–2868.
[29] VOLLER, V. R., BRENT, A. D. & PRAKASH, C. (1989). The modelling of heat, mass and solute transport in solidification systems. *Int. J. Heat Mass Transfer* **32**(9), 1719–1731.
[30] VOLLER, V. R. & SUNDARRAJ, S. (1995) A model of inverse segregation: the role of microporosity. *Int. J. Heat Mass Transfer* **38**, 1009–1018.
[31] VOLLER, V. R. (1997) A similarity solution for the solidification of a multicomponent alloy. *Int. J. Heat Mass Transfer* **40**(12), 2869–2877.
[32] VOLLER, V. R. (1998) A numerical scheme for solidification of an alloy. *Can. Met. Quart.* **37**, 169–177.
[33] VOLLER, V. R., MOUCHMOV, A. & CROSS, M. (2004) An explicit scheme for coupling temperature and concentration fields in solidification models. *Appl. Math. Mod.* **28**, 79–94.
[34] VUŠANOVIĆ, I. & VOLLER, V. R. (2014) Understanding channel segregates in numerical models of alloy solidification: a case of converge first ask questions later. *Mater. Sci. Forum* **790–791**, 74–78.
[35] VUŠANOVIĆ, I. & VOLLER, V. R. (2016) Best practice for measuring grid convergence in numerical models of alloy solidification. *Int. J. Numer. Methods Heat Fluid Flow* **26**, 427–439.
[36] VYNNYCKY, M. & KIMURA, S. (2007) An analytical and numerical study of coupled transient natural convection and solidification in a rectangular enclosure. *Int. J. Heat Mass Transfer* **50**, 5204–5214.
[37] VYNNYCKY, M. & KIMURA, S. (2015) Can natural convection alone explain the Mpemba effect? *Int. J. Heat Mass Transfer* **80**, 243–255.
[38] VYNNYCKY, M. & SALEEM, S. (2017) On the explicit resolution of the mushy zone in the modelling of the continuous casting of alloys. *Appl. Math. Mod.* **50**, 544–568.

https://doi.org/10.1017/S0956792520000091 Published online by Cambridge University Press

[39] VYNNYCKY, M., SALEEM, S. & FREDRIKSSON, H. (2018) An asymptotic approach to solidification shrinkage-induced macrosegregation in the continuous casting of binary alloys. *Appl. Math. Mod.* **54**, 605–626.

[40] WACLAWCZYK, T. & SCHAEFER, M. (2018) Verification of a binary fluid solidification model using semi-analytical solution of 1D heat diffusion equation. *Chem. Process Eng.-Inzynieria Chemiczna i Procesowa* **39**, 85–102.

[41] XIONG, M. & KUZNETSOV, A. (2001) Comparison between lever and Scheil rules for modeling of microporosity formation during solidification. *Flow Turbul. Combust.* **67**, 305–323.

Appendix A Conservation of momentum

The momentum balance in the y-direction for the liquid phase is given by

$$\rho_{\mathrm{l}}\left(\frac{\partial}{\partial t}(\chi v)+\chi v\frac{\partial}{\partial y}(\chi v)\right)=-\chi\frac{\partial p}{\partial y}+\mu\frac{\partial^2}{\partial y^2}(\chi v)+\frac{\mu\chi^2 v}{\kappa(\chi)}+\rho_{\mathrm{l}}g\chi, \tag{A1}$$

where μ is the dynamic viscosity of the liquid phase, p is the pressure, g is the acceleration due to gravity and $\kappa(\chi)$ is the permeability of the mushy region; an often-used expression for this is the Kozeny–Carman relation,

$$\kappa(\chi)=\frac{\kappa_0\chi^3}{(1-\chi)^2}, \tag{A2}$$

where κ_0 is a constant related to the interdendritic arm spacing in the mushy zone. A suitable boundary condition for (A1) would be

$$p=p_{\mathrm{ref}}\quad \text{at } y=y_\infty(t), \tag{A3}$$

with p_{ref} denoting some reference pressure, for example, atmospheric pressure at the surface of the melt.

Setting $U=\chi v$ as before, (A1) becomes

$$\rho_l\left(\frac{\partial U}{\partial t}+U\frac{\partial U}{\partial y}\right)=-\chi\frac{\partial p}{\partial y}+\mu\frac{\partial^2 U}{\partial y^2}+\frac{\mu\chi U}{\kappa(\chi)}+\rho_{\mathrm{l}}g\chi, \tag{A4}$$

and with U already determined from mass conservation, (A4) can be thought of simply as a first-order PDE for p which requires one boundary condition, that is, (A3).

Consequently, the entire formulation accounts for the conservation of mass and momentum in a self-consistent way.

Appendix B Small-time analysis for the solidification of a liquid sphere [21]

In [21], the solidification of a liquid sphere initially at a certain constant temperature V, greater than the fusion temperature, was considered. The temperature field must be calculated for both solid and liquid phases, here denoted by $u(r,t)$ and $v(r,t)$, respectively, which are governed by the linear heat equation. The Stefan condition is applied at the moving interface $r=R(t)$, which represents the solidification front.

https://doi.org/10.1017/S0956792520000091 Published online by Cambridge University Press

The dimensionless model presented in [21] is as follows:

$$\frac{\partial u}{\partial t} = \frac{1}{r^2}\frac{\partial}{\partial r}\left(r^2\frac{\partial u}{\partial r}\right), \quad R(t) < r < 1, \tag{B1}$$

$$\frac{\partial v}{\partial t} = \frac{\kappa}{r^2}\frac{\partial}{\partial r}\left(r^2\frac{\partial v}{\partial r}\right), \quad 0 < r < R(t), \tag{B2}$$

where t represents time and r is the radial distance, subject to

$$u = -1 \quad \text{on } r = 1, \tag{B3}$$

$$u = 0 \quad \text{on } r = R(t), \tag{B4}$$

$$\frac{\partial v}{\partial r} = 0 \quad \text{on } r = 0, \tag{B5}$$

$$v = 0 \quad \text{on } r = R(t), \tag{B6}$$

$$\frac{\partial u}{\partial r} - \kappa\frac{\partial v}{\partial r} = \gamma\frac{\mathrm{d}R}{\mathrm{d}t} \quad \text{on } r = R(t), \tag{B7}$$

where κ is the ratio of thermal diffusivities for liquid and solid phases and γ is the Stefan number. The initial conditions are

$$u = V \quad \text{at } t = 0, \tag{B8}$$

$$R = 1 \quad \text{at } t = 0. \tag{B9}$$

Now, set

$$\xi = \begin{cases} 2 - \frac{r}{R(t)}, & 0 < r < R(t), \\ \frac{1-r}{1-R(t)}, & R(t) < r < 1. \end{cases} \tag{B10}$$

Hence, we have, for $0 < \xi < 1$,

$$(1-R)^2\frac{\partial u}{\partial t} + (1-R)\dot{R}\xi\frac{\partial u}{\partial \xi} = \frac{1}{(1-\xi(1-R))^2}\frac{\partial}{\partial \xi}\left((1-\xi(1-R))^2\frac{\partial u}{\partial \xi}\right); \tag{B11}$$

for $1 < \xi < 2$,

$$R^2\frac{\partial v}{\partial t} + R\dot{R}(2-\xi)\frac{\partial v}{\partial \xi} = \frac{\kappa}{(2-\xi)^2}\frac{\partial}{\partial \xi}\left((2-\xi)^2\frac{\partial v}{\partial \xi}\right). \tag{B12}$$

The boundary conditions are

$$u = -1 \quad \text{on } \xi = 0, \tag{B13}$$

$$u = 0 \quad \text{on } \xi = 1, \tag{B14}$$

$$\frac{\partial v}{\partial \xi} = 0 \quad \text{on } \xi = 2, \tag{B15}$$

$$v = 0 \quad \text{on } \xi = 1, \tag{B16}$$

$$\frac{1}{1-R}\frac{\partial u}{\partial \xi} - \frac{\kappa}{R}\frac{\partial v}{\partial \xi} = -\gamma\frac{\mathrm{d}R}{\mathrm{d}t} \quad \text{on } \xi = 1. \tag{B17}$$

https://doi.org/10.1017/S0956792520000091 Published online by Cambridge University Press

As $t \to 0$, we may now expect $(1-R)\,\dot{R} \sim -\lambda$, where $\lambda > 0$, leading to

$$R\,(t) \approx 1 - (2\lambda)^{1/2}\, t^{1/2}, \tag{B18}$$

with λ still to be determined.

However, with this behaviour for $R\,(t)$, it is clear that (B12) reduces to

$$\frac{\partial v}{\partial \xi} \approx 0, \tag{B19}$$

as $t \to 0$, which means that it is not possible to satisfy both (B6) and (B8). Thus, we need to set

$$\eta = \frac{\xi - 1}{t^{1/2}}, \tag{B20}$$

which is analogous to the boundary layer discussed in Section 3; hence, (B12) gives, for $\eta > 0$,

$$R^2\left(t\frac{\partial v}{\partial t} - \frac{\eta}{2}\frac{\partial v}{\partial \eta}\right) + t^{1/2} R\dot{R}\left(1 - \eta t^{1/2}\right)\frac{\partial v}{\partial \eta} = \frac{\kappa}{\left(1-\eta t^{1/2}\right)^2}\frac{\partial}{\partial \eta}\left(\left(1-\eta t^{1/2}\right)^2 \frac{\partial v}{\partial \eta}\right). \tag{B21}$$

So, as $t \to 0$, (B21) reduces to

$$-\left(\frac{\eta}{2} + \left(\frac{\lambda}{2}\right)^{1/2}\right)\frac{\mathrm{d}v}{\mathrm{d}\eta} = \kappa \frac{\mathrm{d}^2 v}{\mathrm{d}\eta^2}, \tag{B22}$$

whereas (B11) will reduce to

$$-\lambda \xi \frac{\mathrm{d}u}{\mathrm{d}\xi} = \frac{\mathrm{d}^2 u}{\mathrm{d}\xi^2}, \quad 0 < \xi < 1. \tag{B23}$$

(B22) and (B23) will be subject to

$$u = -1 \quad \text{on } \xi = 0, \tag{B24}$$

$$u = 0 \quad \text{on } \xi = 1, \tag{B25}$$

$$v = 0 \quad \text{on } \eta = 0, \tag{B26}$$

$$\left.\frac{\mathrm{d}u}{\mathrm{d}\xi}\right|_{\xi=1} - (2\lambda)^{1/2}\kappa \left.\frac{\mathrm{d}v}{\mathrm{d}\eta}\right|_{\eta=0} = \lambda\gamma, \tag{B27}$$

$$v \to V \text{ as } \eta \to \infty. \tag{B28}$$

As solutions for u and v, we have

$$u = A_1 \mathrm{erf}\left(\left(\frac{\lambda}{2}\right)^{1/2}\xi\right) + B_1, \tag{B29}$$

$$v = A_2 \mathrm{erf}\left(\left(\frac{1}{4\kappa}\right)^{1/2}\left(\eta + (2\lambda)^{1/2}\right)\right) + B_2, \tag{B30}$$

https://doi.org/10.1017/S0956792520000091 Published online by Cambridge University Press

where A_1, B_1, A_2 and B_2 are to be determined, as is λ. We obtain

$$B_1 = -1, \tag{B31}$$

$$A_1 \mathrm{erf}\left(\left(\frac{\lambda}{2}\right)^{1/2}\right) + B_1 = 0, \tag{B32}$$

$$A_2 \mathrm{erf}\left(\left(\frac{\lambda}{2\kappa}\right)^{1/2}\right) + B_2 = 0, \tag{B33}$$

$$\left(\frac{2\lambda}{\pi}\right)^{1/2}\left(\exp\left(-\frac{\lambda}{2}\right)A_1 - \kappa^{1/2}\exp\left(-\frac{\lambda}{2\kappa}\right)A_2\right) = \lambda\gamma, \tag{B34}$$

$$A_2 + B_2 = V, \tag{B35}$$

which results in the usual transcendental equation for λ :

$$\left(\frac{2\lambda}{\pi}\right)^{1/2}\left(\frac{\exp\left(-\frac{\lambda}{2}\right)}{\mathrm{erf}\left(\left(\frac{\lambda}{2}\right)^{1/2}\right)} - \frac{V\kappa^{1/2}\exp\left(-\frac{\lambda}{2\kappa}\right)}{\mathrm{erfc}\left(\left(\frac{\lambda}{2\kappa}\right)^{1/2}\right)}\right) = \lambda\gamma. \tag{B36}$$

Appendix C Comparison with the results in [31]

To validate our method, we compare our results against those given in Figures 3 and 4 in [31]; the comparisons are given in Figure C1. Figure C1(a) shows the results when using the Scheil assumption, whilst Figure C1(b) shows the results when using the lever rule. In both cases, the superheat is taken to be just 1 K. Also, note that these results have been computed using $T_m = 921$ K, which is the value given in [28,31–33], but is neither the value we have given in Table C.1 nor the correct value for the Al–Cu phase diagram which forms the basis of the studies. In fact, using this value for T_m and $T_{eut} = 821$ K, as quoted correctly in [31], leads to $C_{eut} = (T_m - T_{eut})/m \approx 29.5$ wt%, which is lower than the value given in Figure 2. In order to carry out the comparison, we have used the definitions for the similarity variable and mixture concentration given by equations (11) and (28), respectively, in [31]. All of these comments notwithstanding, we can see that very good agreement has been obtained in both sub-plots of Figure C1.

There is, nevertheless, a fundamental difference in the interpretation of this result: in [31], it is intended as being the profile for C for all time as a region of semi-infinite melt solidifies, whereas in our context, it is the small-time solution for an initially finite region of melt. This may help to explain an unusual feature of the result in [31]: namely, that the fully solidified region has uniform composition. Translating back from the similarity variable to physical space variable, this would mean that the solid region has uniform composition; admittedly, this composition is higher than the initial value, as one would expect with inverse segregation, but the profile is still uniform. On the other hand, in our analysis and computations so far, we have found an elevated concentration in the first solid to form at $x = 0$, and further computation for $t > 0$ should show that concentration falls thereafter.

https://doi.org/10.1017/S0956792520000091 Published online by Cambridge University Press

Table C.1. *Parameters for computations for Al-5 wt% Cu*

	Values	Units
c_{pl}	1107	$J\,kg^{-1}\,K^{-1}$
c_{ps}	1107	$J\,kg^{-1}\,K^{-1}$
C_0	5	wt%
g	9.81	ms^{-2}
k_l	100	$W\,m^{-1}\,K^{-1}$
k_s	100	$W\,m^{-1}\,K^{-1}$
k_0	0.17	–
L	0.15	m
m	3.37	K/wt%
T_{cast}	943	K
T_{liq}	916	K
T_m	933	K
T_{sol}	836	K
T_w	621	K
W	0.025	m
κ_0	10^{-11}	m^2
μ	0.007	$kg\,m^{-1}\,s^{-1}$
ρ_l	2400	$kg\,m^{-3}$
ρ_s	2550	$kg\,m^{-3}$
ΔH_f	392,000	$J\,kg^{-1}$

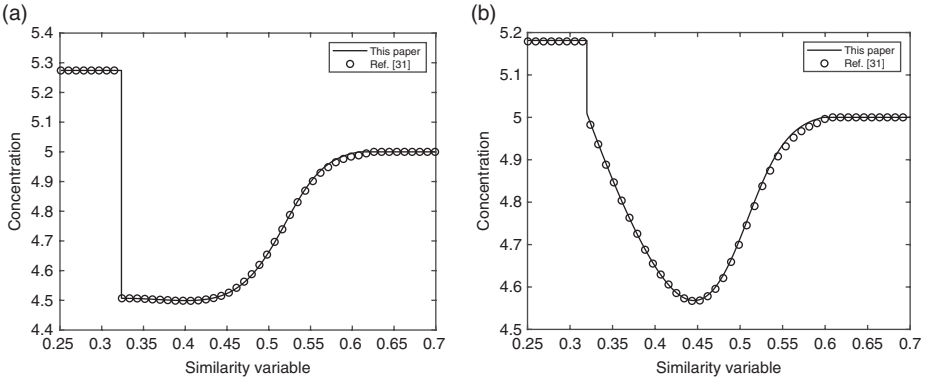


FIGURE C1. Comparison for the mixture concentration with the results in [31] for (a) $\beta = 0$ and (b) $\beta = 1$.

https://doi.org/10.1017/S0956792520000091 Published online by Cambridge University Press